SOP-based DSP Blind Anomaly Detection for Sensing on Deployed Metropolitan Fibers

Leonardo Minelli[(1)], Saverio Pellegrini[(1)], Lorenzo Andrenacci[(1)], Dario Pilori[(1)], Gabriella Bosco[(1)], Luca Della Chiesa[(2)], Alberto Tanzi[(2)], Claudio Crognale[(2)], Roberto Gaudino[(1)]

[(1)]Dipartimento di Elettronica e Telecomunicazioni, Politecnico di Torino. leonardo.minelli@polito.it

[(2)]Cisco Photonics Italy, Vimercate.

Abstract *We propose and compare two DSP anomaly detection schemes based on state of polarization monitoring over 35-km of installed metropolitan fibers. We experimentally evaluate their statistical performance through receiver operating characteristics curves analysis. ©2023 The Author(s)*

Introduction

In recent years, great effort has been dedicated to exploit pre-installed optical fibers to sense mechanical vibrations[1], which has yielded promising outcomes in detecting natural and anthropological activities[2],[3]. In a metropolitan scenario[4],[5], construction and maintenance works can commonly lead to fiber cuts or damages. Anomalous vibration real-time detection is then a key point to determine if an unsafe condition is rising nearby fiber cables, and possibly avoid costs related to replacements or new installations. Moreover, it is fundamental to perform a "blind" detection, i.e. separating normal fiber conditions from hazardous ones without explicit knowledge of anomalous vibrations models. We thus envision in this work an optical fiber-based monitoring system, able to trigger a real-time alarm (with a delay limited to few seconds of processing time) and completely autonomous.

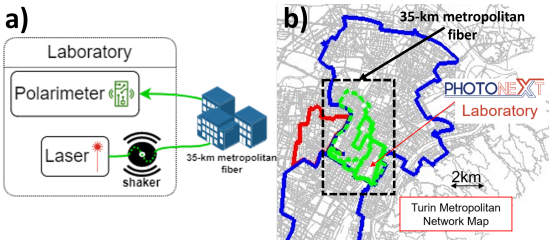

Fig. 1: (a) Map of the 35-km Turin metropolitan fiber in green, (b) block scheme of the experimental set up.

In particular, we investigate DSP solutions for robust anomaly detection through state of polarization (SOP) monitoring on deployed metropolitan fibers. External mechanical perturbations, due to birefringence, induce SOP variations: these can be accurately monitored even using lasers with a broad optical linewidth (i.e., hundreds of kHz)[6]. Polarization is indeed intrinsically stable, and not affected by the noise of the absolute phase of the laser: this makes SOP-based sensing suitable also for commercial coherent transceivers[2]. Recent literature has shown that SOP based Power Spectral Density (PSD) analysis allows to detect events related to mechanical vibrations[2],[3],[7]. In this paper, we propose two DSP schemes for anomaly detection, and we introduce a new signal called SOP-Power Spectral Density Gap (SOP-PSDG), which exploits the PSD of the Stokes parameters to detect low-frequency (<50 Hz) disturbances. We validate these solutions on the experimental setup illustrated in Fig. 1.a, where we induce anomalous vibrations on a short portion of the laboratory fiber connected to the input of a 35-km metropolitan fiber (see Fig. 1.b) deployed in Turin (Italy), and then acquire at its output the SOP using a polarimeter. Fig. 2.a shows the spectrogram of a Stokes parameter (S_3, see next Section) during the SOP acquisition in normal fiber condition, compared to the one (Fig. 2.b) obtained when inducing sinusoidal anomaly (40 Hz) for 10 seconds every minute. By analyzing experimental Receiver Operating Characteristic (ROC) curves[8], we show that anomaly detection leveraging SOP-PSDG outperforms SOP angular speed (SOPAS) thresholding, obtaining an optimal detection accuracy in a wide set of induced mechanical vibrations.

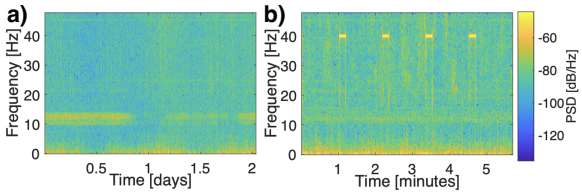

Fig. 2: Experimental S_3 spectrogram (a) in normal fiber conditions (b) with induced 40 Hz sinusoidal vibrations.

Methodology

In this Section, we describe two DSP algorithms for blind anomaly detection: the first considers the SOPAS, while the second is based on the SOP-PSDG. The block schemes of the two algorithms are illustrated in Fig. 3.

They both share a common structure, which processes the SOP evolution acquired from the polarimeter, and the DSP elaborates it to get a real-time alarm signal for anomaly detection. $\mathbf{S} = [S_1, S_2, S_3]$ is the vector containing the Stokes parameters relative to the Cartesian coordinates on the Poincaré sphere. We then refer to $\mathbf{S}[n]$ as the evolution of $\mathbf{S}$ through time, where n is the discrete time index.

In the SOPAS anomaly detector (see Fig. 3.a), the signal $\omega[n]$ is computed as follows,

$$\omega[n] = f_s \cdot \arccos\left(\frac{\mathbf{S}[n-1]\cdot\mathbf{S}[n]}{\|\mathbf{S}[n-1]\|\|\mathbf{S}[n]\|}\right) \quad (1)$$

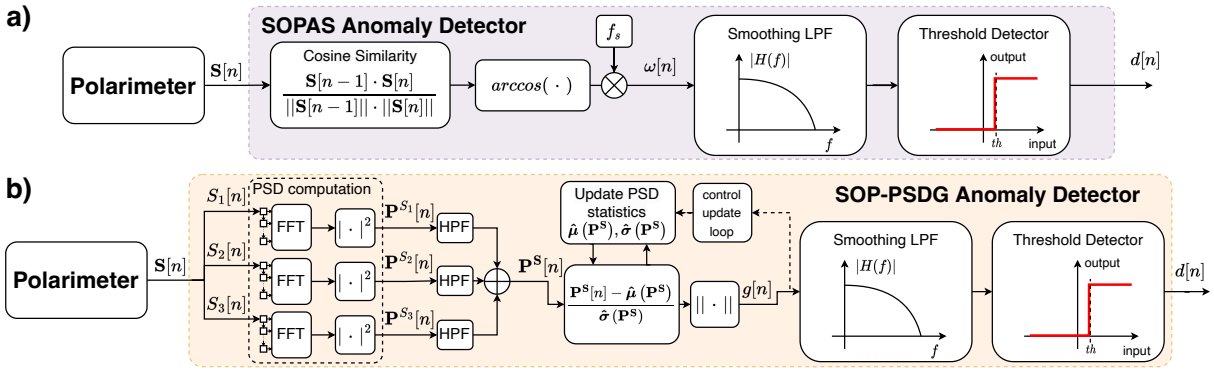

Fig. 3: Schematics of the two anomaly detection algorithms. (a) SOPAS DSP block scheme; (b) SOP-PSDG DSP block scheme.

where f_s is the sampling frequency. $\omega[n]$ represents the magnitude of the SOP angular speed in [rad/s] on the Poincaré sphere, which increases when the fiber is subject to mechanical stresses. The alarm is triggered as the SOPAS exceeds a given value, using a threshold-based detector. Before this, a Low Pass Filter (LPF), implemented as a moving average FIR filter, smooths the signal $\omega[n]$ to ensure signal stability and reduces the risk of false alarms.

In the second DSP scheme (see Fig. 3.b), the SOP-PSDG signal $g[n]$ is designed to detect anomalies in spectral behaviors by evaluating the PSD of the Stokes parameters $S_1[n], S_2[n], S_3[n]$ in real-time and comparing it to its average PSDs values. By quantifying the discrepancy between the current PSD and the past average, unexpected PSD patterns can be identified as anomalies. First, the three $\mathbf{S}[n]$ components are stored into separated digital delay lines. The buffers are exploited to compute the current one-sided power spectral densities (PSD) of the Stokes parameters, represented by the vectors $\mathbf{P}^{S_1}[n]$, $\mathbf{P}^{S_2}[n]$, $\mathbf{P}^{S_3}[n]$, defined as

$$\mathbf{P}^{S_i}[n] = \left[P_1^{S_i}[n], \ldots, P_{\frac{N}{2}+1}^{S_i}[n]\right] \qquad i = 1,2,3 \quad (2)$$

where N is the number of samples stored in the buffers to compute the FFTs. In order to neglect the DSP discrepancies relative to the slow SOP fluctuations in normal conditions, which can broaden over the entire Poincaré sphere, the three PSDs are High Pass Filtered (HPF), by zeroing in each vector the first 2 low-frequency entries. To reduce complexity, the three power spectra are summed element-wise to form a single PSD $\mathbf{P_S}[n]$, representing the magnitude of the SOP power spectral content over the three Poincaré coordinates. Finally, the SOP-PSDG $g[n]$ is computed as the root weighted mean square error (RWMSE) between $\mathbf{P_S}[n]$ and its moving average over time $\hat{\boldsymbol{\mu}}\left(\mathbf{P^S}\right) = \left[\ldots, \hat{\mu}\left(P_k^{\mathbf{S}}\right), \ldots\right]$, as follows:

$$g[n] = \sqrt{\sum_k \frac{1}{\hat{\sigma}\left(P_k^{\mathbf{S}}\right)^2} \left|P_k^{\mathbf{S}}[n] - \hat{\mu}\left(P_k^{\mathbf{S}}\right)\right|^2} \quad (3)$$

where the weights for the RWMSE are given by the vector $\hat{\boldsymbol{\sigma}}\left(\mathbf{P^S}\right) = \left[\ldots, \hat{\sigma}\left(P_k^{\mathbf{S}}\right), \ldots\right]$, whose entries are the element-wise standard deviations over time of the past PSD previously evaluated under normal condition. The element-wise division by $\hat{\boldsymbol{\sigma}}\left(\mathbf{P^S}\right)$ minimizes the penalties caused by the temporal fluctuations of the PSD pattern in normal condition. In practice, the RWMSE computation consists of applying an adaptive normalization to each entry of the vector $\mathbf{P^S}[n]$[9], to then evaluate its euclidean norm to obtain the signal $g[n]$ (see Fig. 3.b). The SOP-PSDG signal is then used for a LPF + Threshold Detector mechanism as for the SOPAS. With this DSP scheme, the SOP-PSDG provides a blind anomaly detector able to keep up in real-time with the non-stationarity of the SOP evolution in normal condition, by updating the PSD statistics $\hat{\boldsymbol{\mu}}\left(\mathbf{P^S}\right)$ and $\hat{\boldsymbol{\sigma}}\left(\mathbf{P^S}\right)$ using current PSD values and the $g[n]$ signal as feedback to the update (see Fig. 3.b).

Experimental Results

The experimental setup is illustrated in Fig. 1.a.

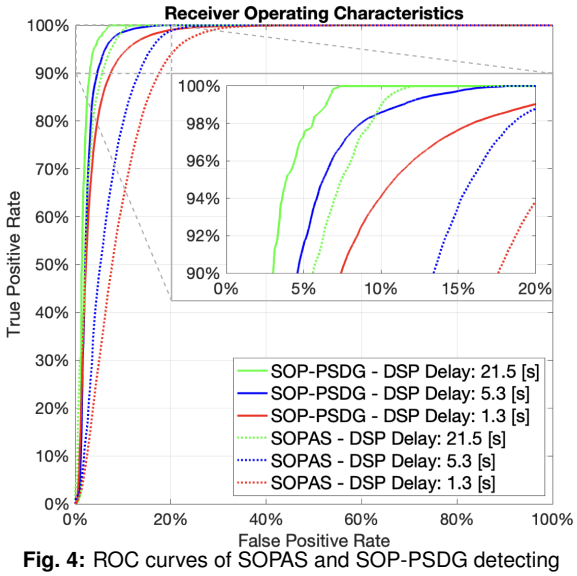

Fig. 4: ROC curves of SOPAS and SOP-PSDG detecting 40Hz-bandwidth vibrations (1.2 Vpp modulation).

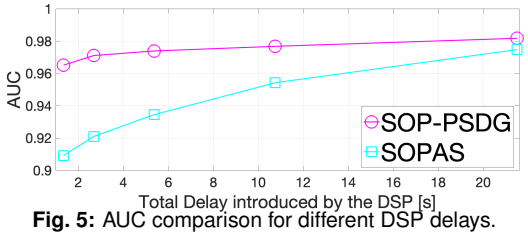

Fig. 5: AUC comparison for different DSP delays.

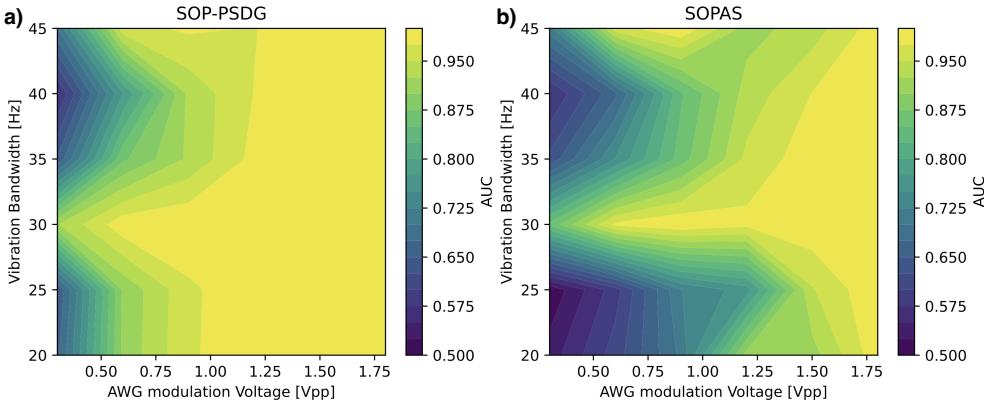

Fig. 6: AUC for different modulation Vpp and bandwidth of the induced vibration (a) using SOP-PSDG (b) using SOPAS

The optical source is a commercial laser, which conveys light inside a 35-km metropolitan single mode fiber deployed around Turin (green path in Fig. 1.b), and outputs light inside a polarimeter, with sampling frequency $f_s = 95.3$ Hz. Anomalies have been induced on fiber by means of a mechanical shaker, over which ~ 1 m of fiber before the metro-span has been glued. An analog waveform generator (AWG) drives the shaker with a low-bandwidth (<50Hz) quasi-Gaussian vibration (i.e., having distribution clipped by the peak-to-peak AWG modulation voltage): this Gaussian-distributed vibration models a generic anomalous stress, emulating the arbitrary nature of real anomalies. To emulate the real-time behavior of the SOP-PSDG, for 20 consecutive times, we performed a 3-minute measurement of SOP evolution without inducing anomalies, followed by 3 minutes of acquisition with shaker-induced vibrations, and then another 3 minutes of anomaly-free acquisition. This approach allowed us to train the average statistics $\hat{\boldsymbol{\mu}}\left(\mathbf{P^S}\right)$ and $\hat{\boldsymbol{\sigma}}\left(\mathbf{P^S}\right)$ on the first acquisition, while the following 2 acquisitions were used for testing the anomaly detectors performance through ROC curves analysis. The ROC curve tracks the probability of correct detection (True Positive Rate) as function of the false alarm probability (False Positive Rate): specifically, by computing the ROC curve's Area Under Curve (AUC) it is possible to assess the accuracy of the detector (perfect detector has AUC=1, random detector has AUC=0.5)[8]. We computed $\omega[n]$ and $g[n]$ (see Fig. 3) to obtain, after the smoothing LPF, the non-thresholded output distributions for the negative and positive anomaly presence hypotheses. Fig. 4 depicts the ROC curves of the SOPAS and SOP-PSDG anomaly detectors for a vibration with 40 Hz bandwidth (1.2 Vpp AWG modulation voltage), for different DSP delays. The delay introduced for the SOPAS DSP accounts for the memory of the smoothing LPF (i.e., the number of FIR taps), whereas in SOP-PSDG the latency is equally split between the FFTs input buffers and the smoothing LPF. The anomaly detector based on SOP-PSDG approaches the upper lefthand corner of the ROC space better than SOPAS: for instance (see inset image in Fig. 4), SOP-PSDG is able within 5.3 seconds to correctly detect (True Positive Rate) 98% of anomalies with less than 8% of false alarms (False Positive Rate), while in the same condition, SOPAS produces over 17% of false alarms. Fig. 5 quantifies the AUC of the ROC curves for both detectors: this shows that SOP-PSDG is significantly better than SOPAS, with an approximately 8% AUC improvement for any delay. Using the same acquisition procedure, several vibration intensities have also been selected by choosing different AWG modulation voltages, from 0.3 to 1.8 Vpp, with a step of 0.3 Vpp. Moreover, the vibration bandwidth has been varied from 20 to 45 Hz with a step of 5 Hz. We specifically test also very weak vibrations (low Vpp and frequency) in order to test the detectors in the harshest conditions. Fig. 6 illustrates the performance of the detectors in terms of AUC by separately evaluating the distributions of the smoothed SOPAS and SOP-PSDG for each anomaly driving condition (with DSP delay set to 5.3 s). It can be observed that the SOPAS-based approach (Fig. 6.b) is able to detect with high confidence (AUC$\sim$1) only anomalies with high intensity (around and bigger than 1.8 Vpp) and vibrations resonating with the experimental setup (30 Hz of noise bandwidth). The SOP-PSDG detector (Fig. 6.a) proves instead to outperform SOPAS in a wide set of different anomalies, resulting a reliable detector even for vibrations down to 1 Vpp (≈ 0.5 mm of maximum fiber displacement): this suggests also a better sensitivity of SOP-PSDG to weak anomalies.

Conclusion and Discussion

We compared 2 SOP-based DSP blind anomaly detectors on deployed metropolitan fibers. Through ROC analysis, SOP-PSDG demonstrates to be a better anomaly detector than SOPAS. The real-time implementation of this DSP algorithm is postponed to future work.

Acknowledgements

This work was carried out under a sponsored research agreement with Cisco Photonics and was partially supported by the European Union under the Italian National Recovery and Resilience Plan (NRRP) of NextGenerationEU, partnership on 'Telecommunications of the Future' (PE00000001 - program 'RESTART'). We also acknowledge the PhotoNext Center at Politecnico di Torino (http://www.photonext.polito.it/)

References

[1] G. Marra, D. M. Fairweather, V. Kamalov, *et al.*, "Optical interferometry-based array of seafloor environmental sensors using a transoceanic submarine cable", *Science*, vol. 376, no. 6595, pp. 874–879, 2022. DOI: 10.1126/science.abo1939. [Online]. Available: https://www.science.org/doi/abs/10.1126/science.abo1939.

[2] A. Mecozzi, C. Antonelli, M. Mazur, *et al.*, "Use of Optical Coherent Detection for Environmental Sensing", *Journal of Lightwave Technology*, pp. 1–8, 2023. DOI: 10.1109/JLT.2023.3252444.

[3] M. Cantono, J. C. Castellanos, V. Kamalov, *et al.*, "Seismic Sensing in Submarine Fiber Cables", in *2021 European Conference on Optical Communication (ECOC)*, 2021, pp. 1–3. DOI: 10.1109/ECOC52684.2021.9605838.

[4] M. Mazur, N. Parkin, R. Ryf, *et al.*, "Continuous Fiber Sensing over Field-Deployed Metro Link using Real-Time Coherent Transceiver and DAS", in *2022 European Conference on Optical Communication (ECOC)*, 2022, pp. 1–4.

[5] E. Ip, Y.-K. Huang, G. Wellbrock, *et al.*, "Vibration Detection and Localization Using Modified Digital Coherent Telecom Transponders", *Journal of Lightwave Technology*, vol. 40, no. 5, pp. 1472–1482, 2022. DOI: 10.1109/JLT.2021.3137768.

[6] A. Mecozzi, M. Cantono, J. C. Castellanos, V. Kamalov, R. Muller, and Z. Zhan, "Polarization sensing using submarine optical cables", *Optica*, vol. 8, no. 6, pp. 788–795, Jun. 2021. DOI: 10.1364/OPTICA.424307. [Online]. Available: https://opg.optica.org/optica/abstract.cfm?URI=optica-8-6-788.

[7] K. S. Y. Skarvang, S. Bjørnstad, R. A. Rørstadbotnen, K. Bozorgebrahimi, and D. R. Hjelme, "Observation of local small magnitude earthquakes using state of polarization monitoring in a 250km passive arctic submarine communication cable", in *Optical Fiber Communication Conference (OFC) 2023*, Optica Publishing Group, 2023, W1J.2. [Online]. Available: https://opg.optica.org/abstract.cfm?URI=OFC-2023-W1J.2.

[8] T. Fawcett, "An introduction to ROC analysis", *Pattern Recognition Letters*, vol. 27, no. 8, pp. 861–874, 2006, ROC Analysis in Pattern Recognition, ISSN: 0167-8655. DOI: https://doi.org/10.1016/j.patrec.2005.10.010. [Online]. Available: https://www.sciencedirect.com/science/article/pii/S016786550500303X.

[9] E. Ogasawara, L. C. Martinez, D. de Oliveira, G. Zimbrão, G. L. Pappa, and M. Mattoso, "Adaptive Normalization: A novel data normalization approach for non-stationary time series", in *The 2010 International Joint Conference on Neural Networks (IJCNN)*, 2010, pp. 1–8. DOI: 10.1109/IJCNN.2010.5596746.